

Linear viscoelastic models

Part III. Start-up and transient flow effects from the molecular weight distribution

Tommi Borg¹

TomCoat Oy, Koskisenkuja 11, 62500 Evijärvi, Finland

Esko J. Pääkkönen

*Tampere University of Technology, Laboratory of Plastics and Elastomer Technology,
P.O. Box 589, 33101 Tampere, Finland*

Start-up and transient shear-stress flows are modelled here using the recently generated constitutive model for linear viscoelasticity of polymers. The relation derived from control theory and the melt calibration procedure has been developed between the relaxation modulus, dynamic viscosity and molecular weight distribution (MWD). This study extends the start-up, decay, and transient effects of linear viscoelasticity on stress and viscosity from the novel viewpoint of the classical Boltzmann superposition principle. We show that shear viscosity is not only a “viscometric function” but also linearly viscoelastic. Moreover, for a constant MWD, application of the method to melt calibration allows interconversions between rheological functions that depend on frequency, shear rate and time. A Cox-Merz rule and power law are also verified. The shear viscosity measurements of well-characterized classical low-density polyethylene (LDPE IUPAC A) with a known MWD were used to obtain time-dependent stress and viscosity transitions. The developed formulas model the start-up situation with an overshoot effect, shear-stress growth, and decay coefficients. Simulations were performed for relaxation modulus measurements at different shear histories defined by the effective viscosity. Dynamic moduli components

¹ To whom correspondence should be addressed.

were modelled, with the results compared with measurement data. As an example of practical applications, capillary flow and injection moulding for producing a mobile-phone cover were modelled to obtain the pressure loss and orientation level for every element in finite element models, which predicted the shrinking and warping of the end products.

Keywords: Polydispersity; Transient viscosity; Shear history; Simulations; Orientation

1. Introduction

Numerous studies (e.g. [1–6]) have modelled the start-up effect using the tube concept of Doi and Edwards for linear polymers. Since polydispersity increases the complexity of modelling, monodisperse polymer melts are generally used in multiscale modelling.

We have used an alternative procedure that starts directly from the molecular weight distribution (MWD) and viscoelastic properties in a polydisperse structure [7,8], which are converted here for shear viscosity and flows with different transitions. This is possible since molecular weight fractions are linearly interrelated by control theory and melt calibration procedures. Our simpler characteristic model rather than our analytical one can be used for these flow simulations, since this choice does not significantly influence the comparison with measured data.

We first present the formulas for steady shear viscosity, and then explain the use of the time-dependent linear transient viscosity rather than the shear stress. A wide range of modelled viscosity functions for the ramp test is presented, the results from which can be used in a simple parallel model to simulate start-up measurements. We introduce a novel

way to explain and sum all shear histories based on the respective effective viscosity using a new version of the classical Boltzmann superposition principle. The importance of the effective relaxation state is highlighted before describing relaxation and other measurements. Finally, the dynamic measurements are modelled and general sources of errors are discussed. Some practical uses are presented in simulations of capillary flow and the filling of injection-moulded parts [9]. This study focuses on shear deformations, and extension cases are not discussed.

The presented principles could aid the development of microstructural tube theories and complete micro–macro relations. Also, the tube concept is needed to model absolute stress and viscosity at some defined shear rate or frequency for the molecular weight fraction presenting a monodisperse polymer.

One of the major aims of this study was to show that the approach based on control theory and melt calibration represents a powerful tool for modelling different viscoelastic flows that remain linear even at rather high strains or shear rates by introducing a novel effective viscosity schema based on a revised Boltzmann principle. The focus of the paper is on deriving the necessary formulas, and hence only brief results are presented. Moreover, our use of a polymer structure with only two user-set factors contrasts with other models that need up to ten such factors, confirming the simplicity and versatility of our method.

Classically, steady simple shear flow $\eta(\dot{\gamma})$ is known as “viscometric flow”. We show using linear control theory and the MWD that this viscometric function is actually linear viscoelasticity. Note that normal forces are not discussed in this paper.

2. Theory

2.1. Characteristic model for shear viscosity

The procedure used to derive the following characteristic formula for shear viscosity is similar to that presented earlier for relaxation modulus [7] and complex viscosity [8]:

$$\log \frac{\eta(\dot{\gamma})}{\eta_0} = -\log \frac{\dot{\gamma}}{\dot{\gamma}_c} \int_{-\infty}^{\log \dot{\gamma}} \left(P' w'(\log \psi) + P'' w''(\log \frac{\psi}{R}) \right) d \log \psi \quad (1)$$

The rheologically effective distribution (RED), $w'(\log \dot{\gamma})$, is a function of shear rate on a logarithmic scale, and the characteristic shear rate, $\dot{\gamma}_c$, is on the order of 1/s. The default ratio of elastic distribution $w'(\log \dot{\gamma})$ to the viscous $w''(\log \dot{\gamma})$ distribution (RED'') was $R = 10^6$, as also used earlier. An alternative model based on a more complex analytical formula inverted for shear viscosity in similar way can be used, but this produced no noticeable difference when modelling the viscoelastic properties over the measured ranges.

A simple relation can be written for the melt calibration, $M(\dot{\gamma})$, as a function of shear rate, where the value of Mf is M at $\dot{\gamma}_1 = 1/s$:

$$M = Mf \left(\frac{\dot{\gamma}_1}{\dot{\gamma}} \right)^{\frac{1}{Hf}} \quad (2)$$

This formula can be used to convert MWD $w(\log M)$ into RED $w'(\log \dot{\gamma})$ or $w'(\log \dot{\gamma}) = w(\log M)$, as needed in Eq. (1).

We used a similar procedure (with the correct selection of Hf and Mf) to express RED $w'(\log \dot{\gamma})$ as a function of time t or frequency ω starting from the same polymer and MWD. Thus, we use MWD $w(M)$ to convert viscoelastic data between different

deformation modes, and thereby explain the general form of the Cox-Merz rule [10]. All presented formulas of principle (except for the approximation formula used for the relaxation spectrum) are commutative, associative and distributive, and thus they exhibit linearity and linear viscoelasticity. In all types of rheological flows, there are different type variables, and the same polymer with a constant MWD. In other words, the same constant MWD $w(M)$ is used as the starting and constant reference point for different linear flow scales of t , ω and $\dot{\gamma}$, which do not give their direct interrelations. Differences arise from Hf and Mf values and also from P' and P'' values depend on the flow type.

2. 2. Boltzmann superposition principle for transient viscosity and history

Transient shear stresses associated with the shear-stress growth coefficient $\sigma^+(t, \dot{\gamma})$ are complicated to model at shear rates ($\dot{\gamma}$), as illustrated in Fig. 1a, and thus we model the *time-dependent transient shear viscosity* $\eta(t, \dot{\gamma})$ at different shear rates. The transient viscosity is a well-known property of many gels and colloids, but is less studied and modelled mainly due to the short-period effects in polymers and instrumentation limitations during measurements, and attempts are made to avoid the effect during steady-state measurements. Subjecting polymers to high shear rates cause shear thinning as a function of time, whereas new low shear rates induce shear thickening. The physical background is related to the probability of chain orientation and degree of entanglement. This transient viscosity can explain some capillary effects and high-speed injection-moulding processes. Start-up stress effects are modelled and verified with measurements in the following section by generated transient viscosity.

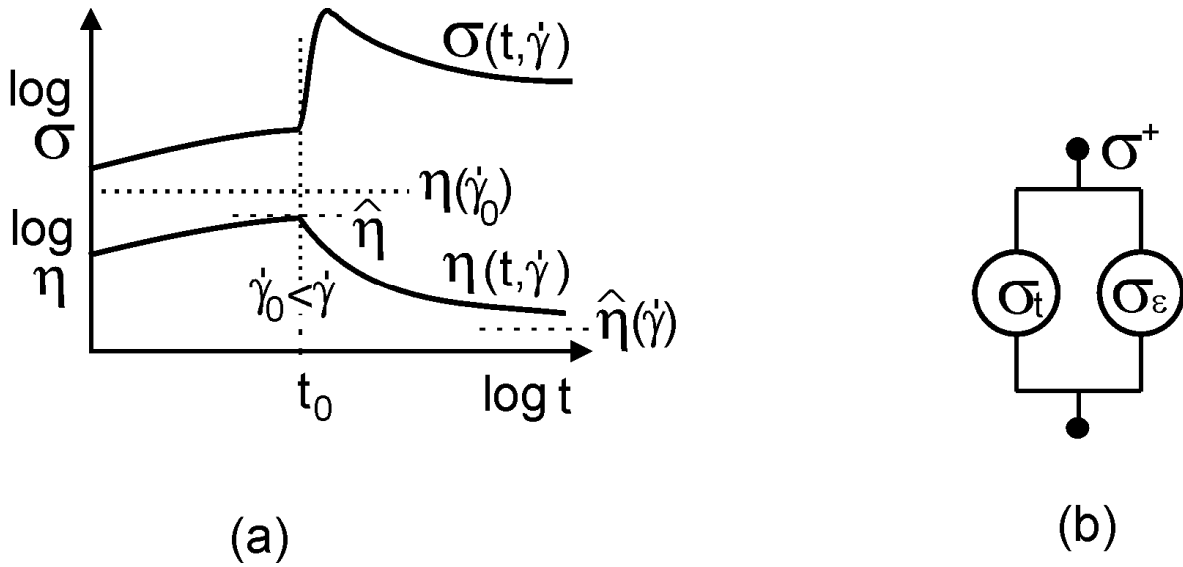


Figure 1. Transient shear-stress and viscosity curves, and schematic of the model for the start-up situation.

a. Graph of time-dependent transient stress $\sigma(t, \dot{\gamma})$ and viscosity $\eta(t, \dot{\gamma})$ during a step increase in the shear rate. The polymer is initially relaxing to steady-state limit $\eta(\dot{\gamma}_0)$, when a new shear rate $\dot{\gamma}$ is imposed at t_0 for effective viscosity $\hat{\eta}$. The viscosity curve appears to be significantly simpler than the stress curve.

b. Schematic of the parallel model for stress growth function σ^+ by time-dependent relaxation stress σ_t^+ and secondary elongation stress σ_ϵ^+ of the shear.

To describe stress and viscosity at different induced shear rates, we use a caret to indicate the *effective* old viscosity $\hat{\eta}$ at $t=t_0$ developed at a shear rate $\dot{\gamma}_0$ or $\hat{\eta}=\eta(t_0, \dot{\gamma}_0)$, which reaches $\lim_{t \rightarrow \infty} [\eta(t, \dot{\gamma}_0)] = \eta(\dot{\gamma}_0)$ in the steady-state situation. Depending on the shear history, effective viscosity $\hat{\eta}$ at time $t=t_0$ may vary considerably from its steady-state limit

$\eta(\dot{\gamma}_0)$. In other words, low-quality measurements might yield true effective viscosity $\hat{\eta}$, which can differ from true steady-state viscosity η .

New imposed shear rate $\dot{\gamma}$ results in the viscosity gradually approaching its limit $\lim_{t \rightarrow \infty} [\eta(t, \dot{\gamma})] = \eta(\dot{\gamma})$. The negative or positive viscosity difference $\Delta\eta = \eta - \hat{\eta}$ approaches zero as a function of normalized relaxation $g(t) = G(t)/G_0$. However, during a constant shear all of the molecules do not relax or orientate to every possible direction (or, at least, the effect is minimal in the perpendicular z direction), and thus we need dimension exponent $D \sim 1/3$ since the relaxation of orientation change is in one direction. The time-dependent transient viscosity is added to the effective viscosity $\hat{\eta}$ at time $t=t_0$: $\eta(t, \dot{\gamma}) = \hat{\eta} + \Delta\eta(t)$. At different shear rates the stress results from the continuous loading of the molecules rather than relaxation, and we get

$$\eta(t, \dot{\gamma}) = \hat{\eta} + (\eta(\dot{\gamma}) - \hat{\eta}) (1 - g(t))^D \quad (3)$$

Now we rewrite the Boltzmann superposition principle for shear viscosity and molecular orientation: the total effect of applying several shear deformations and changes in molecular orientations is simply the sum of their individual effects. Molecular orientation is also related to the effective viscosity, as discussed later. We obtain the general summation from Eq. (3) as follows:

$$\eta(t, \dot{\gamma}) = \hat{\eta} + \sum_{i=1}^N (1 - g(t - t_i))^D \delta \eta(t_i, \dot{\gamma}_i) \quad (4)$$

For continuous changes in viscosity and orientation, this sum is generalized to an integral as

$$\eta(t, \dot{\gamma}) = \hat{\eta} + \int_{-\infty}^t (1 - g(t - \tau))^D \frac{d\eta(\tau)}{d\tau} d\tau \quad (5)$$

Eqs. (3)–(5) can model transient shear viscosity $\eta(t, \dot{\gamma})$ even at high shear rates since $\hat{\eta}$ is used as an absolute starting level with $g(t)$ in a novel manner, where the polymer state can be far from the zero state or starting point.

The Boltzmann superposition principle yields the linear viscoelasticity in a similar way as for all earlier presented formulas for control theory and melt calibration, and we can conclude that we now have linear viscoelasticity starting from the MWD to the transition effects.

2.3. Shear stress growth and decay coefficients

In the start-up situation, shear stress growth function $\sigma^+(t, \dot{\gamma}) \equiv \sigma$ and respective shear stress growth coefficient $\eta^+(t, \dot{\gamma}) \equiv \frac{\sigma^+}{\dot{\gamma}}$ can be expressed according to nomenclature [11] as approaching its steady-state limit as

$$\lim_{t \rightarrow \infty} [\eta^+(t, \dot{\gamma})] = \eta(\dot{\gamma}) \quad (6)$$

The application of a shear stress to a well-relaxed polymer may result in overshoots of stress growth coefficient $\eta^+(t, \dot{\gamma})$ and the molecular elongation forces. There are two types of stresses for stress growth function σ^+ : (1) time-dependent relaxation stress σ_t^+ and (2) the shear rate growth, which generates elongation stress σ_ε^+ for chains before a new orientation and steady state is reached. These forces act in parallel as shown in Fig. 1b, and we can write a simple formula for σ^+ that is analogous to parallel resistors in a electric circuit:

$$\frac{1}{\sigma^+} = \frac{1}{\sigma_t^+} + \frac{1}{\sigma_\varepsilon^+} \quad (7)$$

In Eq. (7) we can use Eq. (3) for transient viscosity $\eta(t, \dot{\gamma})$, formulas $\gamma = \dot{\gamma}t$ and $\sigma = \eta\dot{\gamma}$, and simple algebraic conversions such as multiplying by $\dot{\gamma}$ to obtain

$$\frac{\dot{\gamma}}{\sigma^+} = \frac{1}{\eta(t, \dot{\gamma})} + \frac{1}{\eta(t, \dot{\gamma})\dot{\gamma}_\varepsilon t} \quad (8)$$

Since elongation stress $\sigma_\varepsilon^+ = \eta_E \dot{\varepsilon}$ is a function of Hencky strain rate $\dot{\varepsilon}$ and Trouton viscosity η_E , we have to convert these into a function of the shear rate. In the linear case $\eta_E(\dot{\varepsilon}) = 3\eta(\dot{\gamma})$ and the stress can be written as $\sigma_\varepsilon^+ = \eta_E \dot{\varepsilon} = \eta\dot{\gamma}_\varepsilon$, where the extension shear rate is $\dot{\gamma}_\varepsilon = 3\dot{\gamma}$ and is lower at somewhat higher rates in the non-linear case.

After simple algebraic conversions, this finally yields the formula for start-up flow

$$\eta^+(t, \dot{\gamma}) \equiv \frac{\sigma^+}{\dot{\gamma}} :$$

$$\eta^+(t, \dot{\gamma}) = \frac{\eta(t, \dot{\gamma})\dot{\gamma}_\varepsilon t}{\dot{\gamma}_\varepsilon t + 1} \quad (9)$$

For shear-stress decay coefficient $\eta^-(t) \equiv \frac{\sigma^-}{\dot{\gamma}_\varepsilon}$ and after the cessation of steady shear, we can use classical formula

$$\eta^-(t) = \int_t^\infty G(s) ds \quad (10)$$

All of these functions need viscosity measurements as a function of the shear rate to generate the relaxation modulus and wide-ranging viscosity flow.

2.4. Simulations for the relaxation modulus

The measurement of relaxation modulus requires at least two steps, including simulating the shear history and the shear of the initial ramp. We rewrote the procedure presented in our earlier papers to find effective viscosity $\hat{\eta}$ and effective zero relaxation modulus \hat{G}_0 at $t=t_0$ instead of classical zero modulus G_0 . The polymer is no longer fully relaxed after a step strain is used to measure the relaxation modulus, and hence \hat{G}_0 is lower than its conventional value G_0 . The effective G_0 , \hat{G}_0 , is determined directly by setting $t>0$ for conventional relaxation modulus $G(t)=\hat{G}_0$ or by using the respective effective shear rate, $\hat{\gamma}_0$, which gives the respective effective zero viscosity $\hat{\eta}_0 = \eta(\hat{\gamma}_0)$. Eq. (11) can be used to obtain the respective \hat{G}_0 . The internal effective zero relaxation modulus of the polymer, \hat{G}_0 , tends to G_0 during a zero shear situation: $\lim_{t \rightarrow \infty} [\hat{G}_0(t)] = G_0$.

We used standard simple numerical feedback fitting procedures (e.g. bracketing) while solving Eq. (11) by testing the new effective \hat{G}_0 values to obtain the formula for effective zero viscosity $\hat{\eta}_0$:

$$\hat{\eta}_0 = \int_{-\infty}^{\infty} t \hat{G}_0 g(t) d \log t \quad (11)$$

where $\hat{\eta}_0 = \eta(\hat{\gamma}_0)$ is determined by the respective effective shear rate $\hat{\gamma}_0$. In most cases the polymer still has some orientation and is not in a fully relaxed state, and thus $\eta_0 > \hat{\eta}_0$ with $\hat{\gamma}_0 > 0$ for the polymer melt, with Eq. (11) yielding $\hat{G}_0 < G_0$. All of the shear history can be explained by $\hat{\eta}$ or with the respective effective shear rate $\hat{\gamma}$ for steady-state viscosity $\eta(\hat{\gamma})$.

The effective viscosity is the same as the respective steady-state limit at a constant shear rate or $\dot{\gamma} = \hat{\gamma}$ and $\hat{\eta} = \eta(\dot{\gamma}) = \eta(\hat{\gamma})$.

Now we use relaxation function $G(t, \hat{\gamma}) = G_0(t) - \Delta G_0(t)$, where $G_0(t)$ is the theoretical relaxation modulus for a fully relaxed state, and $\Delta G_0(t) = G_0(t) - \hat{G}_0(t)$ with $\hat{G}_0(t) = \hat{G}_0 g(t)$. The principle is similar to that presented for the transient viscosity in Eq. (3):

$$G(t, \hat{\gamma}_0) = G_0(t) + (G_0(t) - \hat{G}_0(t)) \left(1 - \frac{G_0(t)}{G_0}\right)^D \quad (12)$$

Relaxation function $G(t, \hat{\gamma})$ can be converted to a standard imposed-ramp relaxation function $G(t, \gamma)$ as a function of strain using the information in Fig. 3 if the shear history, implied duration of strain and amount of strain are known.

Most attempts to model $G(t, \gamma)$ using constitutive equations lead to time-strain separability functions [12], which are generally not derived from fundamental principles. The form of these functions provides theoretical simplicity and practical convenience for modelling constitutive equations. Nevertheless, separability is violated in short-time responses immediately after the application of a step strain. Our basis is the new *time-rate* separability shown in Eq. (3) for transient viscosity and for the relaxation function in Eq. (12). This new approach allows any time window to be modelled even in a highly orientated non-relaxed state.

When a large step strain γ is applied for a long time before relaxation, respective effective shear rate $\hat{\gamma}$ is close to the steady-state shear rate used for deformation. In the opposite case with a high shear rate, the polymer will not have reached the steady state, and

relaxation will produce higher forces. Fortunately, Eq. (3) yields effective shear rate $\hat{\gamma}$ and viscosity $\hat{\eta}$ to $G(t, \hat{\gamma})$ at any time, and converts it further to $G(t, \gamma)$.

2.5. Partitioning into dynamic moduli components G' and G'' and transition effects

Finally, we model the dynamic measurements and compare with the measured dynamic storage G' and loss G'' moduli. We convert the characteristic equation presented previously [8] in Eq. (7) for complex viscosity algebraically into the following exponential form:

$$\eta_c^*(\omega) = \eta^*_0 \exp\left(-P' \log\left(\frac{\omega}{\omega_c}\right) \int_{-\infty}^{\log \omega} w' \log \omega d \log \omega - P'' \log\left(\frac{\omega}{\omega_c}\right) \int_{-\infty}^{\log \omega} w'' \left(\log \frac{\omega}{R}\right) d \log \omega\right) \quad (13)$$

Equation (13) comprises two components that can be expressed in complex notation as

$e^{-P'(\omega)-P''(\omega)} = e^{-P'(\omega)} e^{-P''(\omega)}$, where functions $P'(\omega)$ and $P''(\omega)$ are given by

$$P'(\omega) = P' \log\left(\frac{\omega}{\omega_c}\right) \int_{-\infty}^{\log \omega} w' (\log \omega) d \log \omega \quad (14)$$

$$P''(\omega) = P'' \log\left(\frac{\omega}{\omega_c}\right) \int_{-\infty}^{\log \omega} w'' \left(\log \frac{\omega}{R}\right) d \log \omega \quad (15)$$

and we partition Eq. (13) into storage and loss modulus components, where complex modulus $G^*_0 = \eta^*_0 \omega$ is given by

$$G'(\omega) = G^*_0 \frac{P'(\omega)}{\sqrt{P'^2(\omega) + P''^2(\omega)}} \quad (16)$$

$$G''(\omega) = G^*_0 \frac{P''(\omega)}{\sqrt{P'^2(\omega) + P''^2(\omega)}} \quad (17)$$

This partition could also easily be applied to the shear viscosity and relaxation modulus, or using the computed dynamic storage G' and loss G'' moduli as measured data for the familiar deconvolution procedure to obtain $G(t)$. However, difficulties are encountered when modelling certain polyolefin measurements at low temperatures due to long transition time effects as discussed in Section 3.

2.6. Power law

For simplicity, we set up a very practical characteristic *polymer structure function* $P_c(\dot{\gamma})$:

$$P_c(\dot{\gamma}) = \int_{-\infty}^{\log \dot{\gamma}} \left(P' w'(\log \psi) + P'' w''(\log \frac{\psi}{R}) \right) d \log \psi . \quad (18)$$

In computer simulations it is much more convenient to use the short form of the equation, which gives us a simple power-form formula to Eq. (1) and approximates the true molecular orientation level and state:

$$\eta(\dot{\gamma}) = \eta_0 e^{-P_c(\dot{\gamma}) \log \frac{\dot{\gamma}}{\dot{\gamma}_c}} . \quad (19)$$

Setting the characteristic shear rate as $\dot{\gamma}_c = 1/s$ yields a simple power law for the shear viscosity as a function of shear rate:

$$\eta = \eta_0 |\dot{\gamma}|^{-P_c(\dot{\gamma})} , \quad (20)$$

where $P_c(\dot{\gamma})$ is a function of shear rate as $e^{-P_c \log |\dot{\gamma}|} = |\dot{\gamma}|^{-P_c(\dot{\gamma})}$. It is worth noting that the relation for power-law index n is $P_c(\dot{\gamma}) = 1 - n$ at high shear rates. According to the used principle, $P_c(\dot{\gamma})$ indicates the influence of effective viscous $w''(\dot{\gamma})$ and also changes in the elastic $w'(\dot{\gamma})$ distribution REDs, which besides incorporating the chain structure relates the

orientation and degree of entanglement as functions of the shear rate. Since power-law index n is a constant factor for a polymer sample within the measurement range, it relates only to the average chain structure and entanglement probability.

2.7. Simulating the molecular orientation during transition effects

Whilst it is important to model the shear stress and viscosity, it is equally important to model the molecular orientation during these transitions. Orientation levels represent the memory and source of viscosity. The exponent form for characteristic polymer structure function $P(\dot{\gamma})=P'(\dot{\gamma})+P''(\dot{\gamma})$, which in principle is shown in Eq. (18), is related to the orientation level. This yields an effective shear viscosity $\hat{\eta}=\eta_0 |\dot{\gamma}|^{-P(\dot{\gamma})}$ according to Eq. (1) modified by some simple algebraic conversions. During shear rate variations and induced shear history, Eq. (20) yields the effective viscosity $\hat{\eta}$ for respective effective polymer structure function \hat{P} :

$$\hat{P} = -\frac{1}{|\dot{\gamma}|} \log \frac{\hat{\eta}}{\eta_0} \quad (21)$$

Since $0 < \hat{P} < 1$ normally holds in the characteristic model, the effective exponent \hat{P} is more descriptive in absolute percentage form ($\hat{P} \% = 100 \hat{P}$) or even in relative form:

$$\hat{P}_{\text{REL}} \% = 100 \hat{P} / \hat{P}_{\text{MAX scale}} \quad (22)$$

2.8. Cox-Merz rules

The original Cox-Merz rule [10] $\eta(\dot{\gamma}) = |\eta^*(\omega)|_{\omega=\dot{\gamma}}$ and its extended or modified variations can be explained using the presented principle. Different flow scales of t , ω and $\dot{\gamma}$ do not

have direct physical interrelations. Sometimes Cox-Merz rules hold and sometimes they fail completely, and this has been investigated by many studies. It is not always possible to find the correct MWD from control theory, but only on very rarely occasions has the viscoelastic properties not been modelled accurately. For these different flow types the same polymer and corresponding MWD are used, but the flow deformations differ.

We can use the MWD obtained from the melt calibration to generate REDs as a function of shear rate, $\dot{\gamma}$, or $w'(\log M) = w(\log \dot{\gamma})$ or as a function t and ω , using different P' and P'' constants and effective zero states $\hat{\eta}_0, \hat{\eta}^*_0$, or \hat{G}_0 depending on the flow type. Thus, we can convert viscoelastic data between different deformation modes, and thereby explain Cox-Merz rules in the case of P', P'' and the same zero states:

$$w(M) = \left\langle \left| \eta(\dot{\gamma}) \right|_{\eta_0, P', P''} ; \left| \eta^*(\omega) \right|_{\eta^*_0, P', P''} ; \left| G(t) \right|_{G_0, P', P''} \right\rangle \quad (23)$$

In other words, the same constant (MWD $w(M)$) is used as the starting and reference point for different REDs and flow scales of t , ω and $\dot{\gamma}$, as shown in Fig. 2. When P', P'' and the zero states are the same, Cox-Merz rules hold. The use of frequency ω (1/s) or angular frequency ω (rad/s) could also be adjusted by structural factor Mf to obtain the correct fit, with in principle a similar being taken with modified or extended Cox-Merz rules.

Our presented principle based on melt calibration is much more versatile, and allows the conversion to any linear scales by adjusting Mf and scale units using conversion factor Hf .

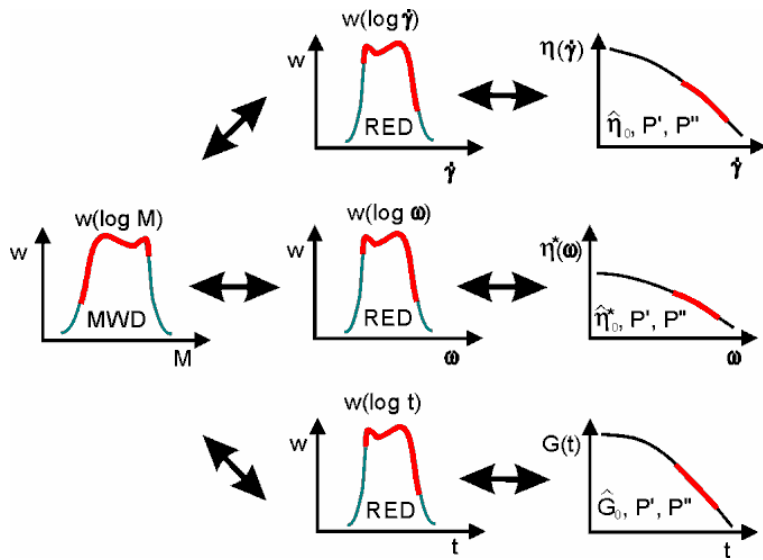


Figure 2. Using the presented method of melt calibration yields the MWD that remains the same for different flows and scales. Thicker lines are measured data. The original Cox-Merz rule holds if P' , P'' and the zero states are the same.

3. Experimental

3.1. Procedure, test polymers and constants

Flow simulations are presented in different ways and from different viewpoints, and are compared with measurements if there are data available. Control theory is known to be theoretically capable of modelling a *partially observed system*. We first compare the results of some transition viscosity and start-up and stress decay coefficient modelling with measurements shown in Figs. 3–6. The importance of relaxation state during relaxation and dynamic moduli measurements is also presented in Fig. 7. Finally, as an example of practical applications, simulations of the orientation during capillary flow and the filling phase of an injection-moulded mobile-phone cover are presented.

Most of the computations were performed on a standard PC using the RheoPower software package and the characteristic models described by Eq. (1) for shear viscosity. Orientation simulations were carried out with *Datapower* server software and the version from third part of the simulation client software *cmv6*. The used polymer IUPAC A, a well-characterized low-density polyethylene (LDPE) as described by Meissner [13,14].

For the dynamic simulation shown in Fig. 8, and for the orientation simulations of capillaries and the filling of injection-moulded parts shown in Figs. 9 and 10, for which dynamic measurements at different temperatures were also needed, BASF gave us permission to use their oscillating-rheometer data for Lupolen 1840H LDPE (the qualitatively similar rheological properties of IUPAC A LDPE) measured at temperatures from 130°C to 250°C. The complex viscosity [13] and shear viscosity flow curves of this polymer are very similar to those of the shear viscosity measurements by Laun [15].

The default value of $R = 10^6$ for distance was set for the Rouse shear range distribution. The oscillation rheometer data indicated that $Mf = 37,800$ g/mol and $Hf = 2.05$, and the capillary data indicated $Mf = 20,000$ g/mol and $Hf = 2$. The average molecular weight M_w for IUPAC A LDPE was measured originally to be 472,000, and the polydispersity index, M_w/M_n , was 24.9. We therefore used $M_w = 480,000$ and $M_w/M_n = 25$ in our modelling, and $M_w = 235,000$ g/mol and $M_w/M_n = 14.1$ were used for 1840H LDPE.

Please note that the values of P' and P'' were found from the viscosity fitting procedure, and no *ad hoc* constants or values were used except for the results presented in Fig. 10. A constant characteristic frequency of $\omega_c = 1/s$, characteristic shear rate $\dot{\gamma}_c = 1/s$, and characteristic time of $\tau_c = 10^{-6}$ s were used. Dimension exponent D had a value of 1/3

in all computations. The main functions and characteristics of these computations are listed in Table 1.

TABLE 1. Main functions and characteristics of all computations.

Fig.	In ^a	Out ^b	T^c	M_w^d	M_w/M_n^d	Mf^e	Hf^e	P'^f	P''^f
3	$\eta(\dot{\gamma})$	$\eta(t, \dot{\gamma})$	150	480,000	25.0	20,000	2	0.41	0.18
4	$\eta(t, \dot{\gamma})$	$\eta^+(t, \dot{\gamma})$	150	480,000	25.0	20,000	2	0.41	0.18
5	$\eta(t, \dot{\gamma})$	$\eta^+(t, \dot{\gamma})$	150	480,000	25.0	20,000	2	0.41	0.18
6	$G(t)$	$\eta^-(t)$	150	480,000	25.0	37,800	2.05	0.38	0.20
7	$\hat{\eta}_0$	$G(t, \hat{\gamma}), G(t, \gamma)$	150	480,000	25.0	20,000	2	0.39	0.08
8	$\eta^*(\omega)$	G', G''	200	237,000	14.0	50,652	2.05	0.37	0.25
9	$\eta(t, \dot{\gamma})$	$\hat{P} \%$	150	240,000	14.6	20,000	2	0.42	0.26
10	$\eta(t, \dot{\gamma})$	$\hat{P} \%$	130– 250	240,000	14.6	20,000	2	0.32– 0.44	0.15– 0.27

^aViscoelastic function used as a data source.

^bModelled viscoelastic function.

^cTemperature (°C).

^dAverage molecular weight M_w (g/mol) and polydispersity index M_w/M_n .

^eStructural value Mf and conversion factor Hf .

^fElasticity and viscosity values P' and P'' .

The RheoAnalyzer (Vis-MWD) module was used to compute MWD for Fig. 8 and to model complex moduli. Other figures were produced using the RheoDeveloper (MWD-Vis) module with capillary measurements at 150°C. Complex viscosities measured at

different temperatures were used for the temperature dependence of η_0 in Fig. 10 in a similar way to using P' and P'' constants by simple linear algebra formulas. The generated data files were transferred to the separate DataPower Server program. The procedures used are not very sensitive to the form of the MWD used when modelling viscoelastic properties, unlike when the MWD is detected from viscoelastic measurements.

3.2. *Simulations of transient, start-up and cessation viscosities, and relaxation and dynamic moduli*

We modelled the transient viscosity, which was subsequently used for simulating start-up, cessation and relaxation measurements. We began with the known MWD of IUPAC A LDPE, and used the MWD-Vis mode of the software.

After the relation between the RED (converted from the MWD) and the measured shear viscosity was accurately determined, we generated relaxation modulus $G(t)$ according to measurements and fitting with Eq. (9) reported by [7]. Dynamic viscosity measurements were used to compute the MWD, and modelling $G(t)$ at a fully relaxed state G_0 without any shear history at an effective shear rate $\hat{\gamma} = 10^{-6}/s$ gave the zero viscosity $\eta_0 = \hat{\eta}_0$. The highest fractions of the MWD set this zero rate point during viscosity modelling. Equation (3) could be used to generate transient viscosity $\eta(t, \dot{\gamma})$ from the steady and effective shear rate $\dot{\gamma}_0 = \hat{\gamma} = 1/s$ at $t = t_0$ for new shear rates $\dot{\gamma}$ ranging from 0.00001/s to 100000/s, as shown in Fig. 3. Since it is difficult to measure the transient viscosity, the results were verified indirectly using start-up measurements.

Although making oscillating rheometer measurements constitutes a different type of experiment, there are similarities when using a high orientation degree at high frequency. Figure 3 shows why it is better to use a rapid-upward-frequency-sweep test with an oscillating rheometer set at its factory default sensitivity, since then the steady state is reached more quickly at each frequency. If the acceptance criterion for a steady state has been risen, then the direction of the frequency sweep is not very important. Rapid effects in polymer melts have not been measured due to limitations of measurement devices, but similar results have been found for polymer solutions, for which the timescale of transitions is longer [16].

Logically it can be assumed that for transient viscosity $\eta(t, \dot{\gamma})$ during high shear rates or with relaxation function $G(t, \hat{\gamma})$ in a strongly non-relaxed state it should be possible to use $\hat{G}_0(t) = \hat{G}_0 g(t)$ with a small \hat{G}_0 value in Eq. (3) or (12) instead of G_0 , since the polymer is highly oriented. However, our simulation tests revealed that it is not the case.

All chains can give response for changes in shear rate or deformation. Non-linearities are induced by pressure, density changes or local friction heating for higher rates of true flows, and these are not discussed here since our linear models do not hold.

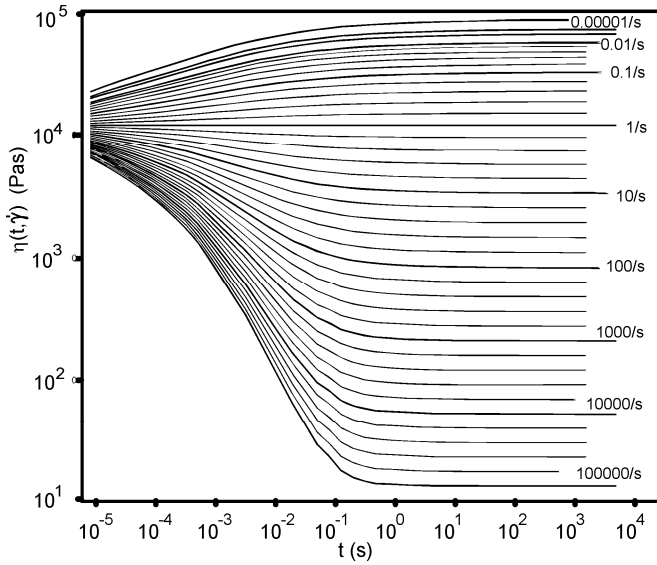


Figure 3. Modelled transient viscosity $\eta(t, \dot{\gamma})$ over a wide range of $\dot{\gamma}$ values for IUPAC A LDPE at 150°C from the steady and effective shear rate $\dot{\gamma}_0 = \hat{\gamma} = 1/s$ at $t = t_0$.

We used Eq. (9) for start-up simulations of the shear-stress growth coefficient $\eta^+(t, \dot{\gamma})$ and used effective shear rates $\hat{\gamma}$ ranging from $10^{-6}/s$ to $10^{-1}/s$. The viscosity at a steady rate $\dot{\gamma} = 10^{-6}/s$ was the same as zero viscosity $\eta_0 = \hat{\eta}_0$, indicating that the polymer was fully relaxed and that $\hat{\gamma} = 10^{-6}/s$ also. This state is difficult to achieve in practice, as indicated by the results being closer to the measured values with a higher starting effective $\hat{\gamma}$. Measurements were made over 30 years ago by Weissenberg Rheogoniometers [14], when inertia forces and other instrumentation errors before $t=1$ s were higher than for modern instruments. Those studies also found that strain resulted in distortions on a longer timescale, on the order of $t=100$ s. Thus, the measured overshoot may be too sharp. Equation (9) indicates that at longer times the limiting viscosity $\eta^+(t, \dot{\gamma})$ corresponds to the

shear viscosity η at a rate $\dot{\gamma}=1/s$, but the values in Fig. 4 are lower due to distortions induced by the applied strains and used linear model by setting $\dot{\gamma}_\varepsilon = 3\dot{\gamma}$ in Eq. (9).

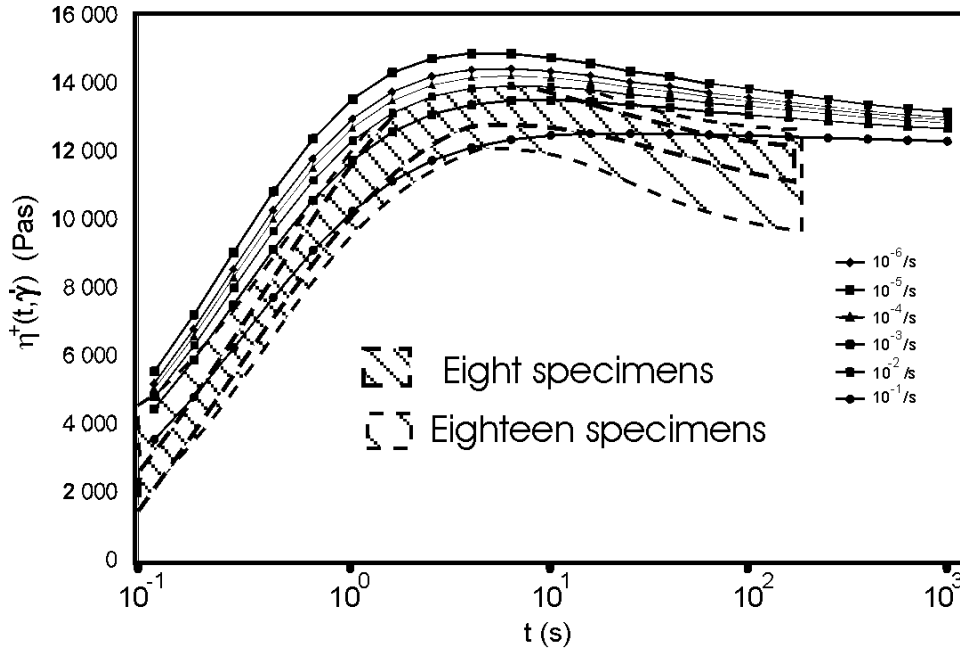


Figure 4. Measured and modelled start-up $\eta^+(t, \dot{\gamma})$ viscosity curves of IUPAC A LDPE at 150°C. The specimen was measured at 18 laboratories (wide hatching), and the results from the 8 most reliable specimens (narrow hatching) are close to the modelled data up to 100 s. The discrepancy for $t > 100$ s is attributable to measurement limitations and distortions induced by the applied strains.

Transient viscosity $\eta(t, \dot{\gamma})$ in Fig. 3 initially decreases monotonically for a higher imposed shear rate, but the start-up viscosity ($\eta^+(t, \dot{\gamma}) = \frac{\sigma^+}{\dot{\gamma}} = \frac{\eta(t, \dot{\gamma})\dot{\gamma}}{\dot{\gamma}}$) at a new higher shear rate can still generate overshoot.

Figure 5 shows the same simulated results for $\eta^+(t, \dot{\gamma})$ for a fully relaxed polymer on a wider range of new shear rates. Also high new rates are modelled by linear model by setting $\dot{\gamma}_\varepsilon = 3\dot{\gamma}$ in Eq. (9) and may be found differences in real obtained values. The computed results include the curve obtained using relaxation modulus $G(t)$ for the

conventional equation $\eta^+(t) = \int_0^t G(s) ds$.

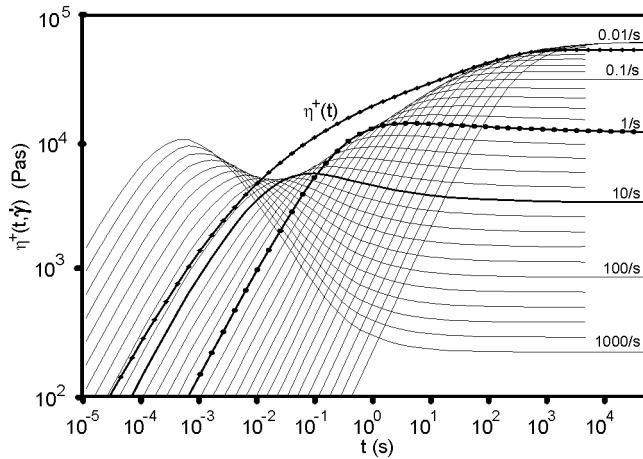


Figure 5. Modelled start-up $\eta^+(t, \dot{\gamma})$ viscosity curves of IUPAC A LDPE at new induced lower and higher shear rates. The lower thick line corresponds to the induced $\dot{\gamma} = 1/s$ shear rate, as shown in Fig. 4. The upper thicker line was calculated from the relaxation modulus using the classical equation.

Figure 6 shows the modelled shear-stress decay coefficient $\eta^-(t)$ according to Eq. (10) after the cessation of a steady shear. We multiplied the original normalized reduced stress viscosity reported by Meissner [13] for IUPAC A LDPE at 150°C by $\eta_\infty^- = 19628$ Pas, which they did not include. The measurements again differ from the

modelling results for $t < 1$ s, possibly due to instrumentation limitations. However, modern rheometers are able to measure the viscosity better at the beginning of the runs.

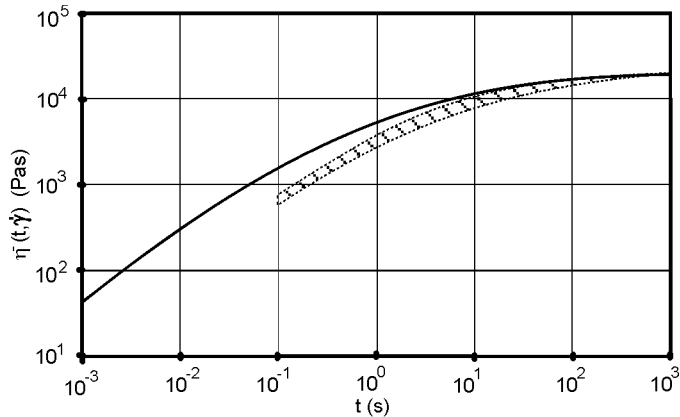


Figure 6. Modelled shear-stress decay coefficient $\eta^-(t)$ after the cessation of steady shear.

The measurements of IUPAC A LDPE at 150°C are indicated by the hatched area.

Relaxation modulus $G(t, \dot{\gamma})$ was simulated for the polymer with a different shear history for the respective shear rate at t_0 . Not only the shear history but also the imposed-ramp strain affects the molecular orientation, and during practical tests the polymer always exhibits a higher effective shear rate $\hat{\gamma} > 10^{-6}/s$, giving a lower effective viscosity $\hat{\eta}_0 < \eta_0$ for shear-thinning polymers. This gives a lower effective computed relaxation modulus $\hat{G}_0 < G_0$ according to Eq. (11), and the results are shown in Fig. 7 for effective shear rate $\hat{\gamma}$ giving the respective $\hat{\eta}_0$ and thus \hat{G}_0 values.

Interpolation of the measured relaxation modulus at $t=0.1$ s indicates that the correspondence is closest for $\hat{\gamma}=0.0025/s$, which does not indicate a well-relaxed polymer and is much more than the fully relaxed state at $\hat{\gamma}=10^{-6}/s$.

More relaxation measurements could be simulated using a chart for $\eta(t, \dot{\gamma})$ similar to that shown in Fig. 3 but starting from a steady shear rate $\dot{\gamma} = \hat{\dot{\gamma}} = 10^{-6}/\text{s}$. Knowledge of the imposed strain and time would make it possible to simulate also the polymer relaxation state before relaxation and determine the standard imposed-ramp relaxation function $G(t, \gamma)$.

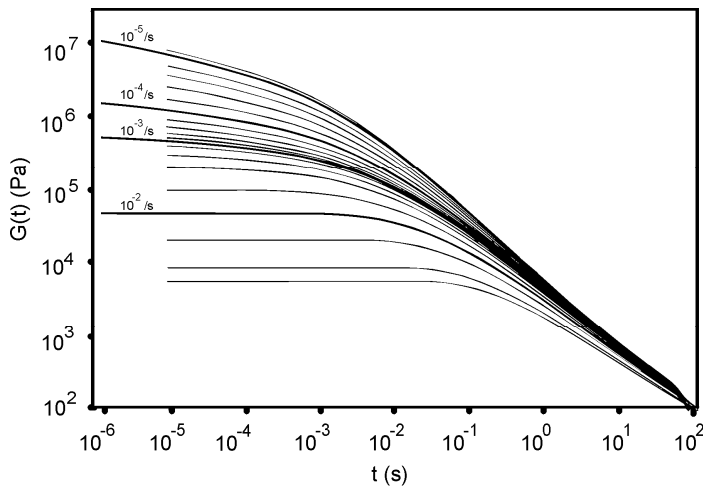


Figure 7. Simulated relaxation modulus $G(t, \hat{\dot{\gamma}})$ at different effective shear rates related to effective zero relaxation modulus \hat{G}_0 and also for more familiar $G(t, \gamma)$ tests.

Finally, we modelled the dynamic measurements and compare the results with measured the dynamic storage G' and loss G'' moduli with measurements according to Eqs. (16) and (17). We did not have dynamic data for the original IUPAC A LDPE, so we instead used the qualitatively similar rheological properties of 1840H LDPE in the simulations.

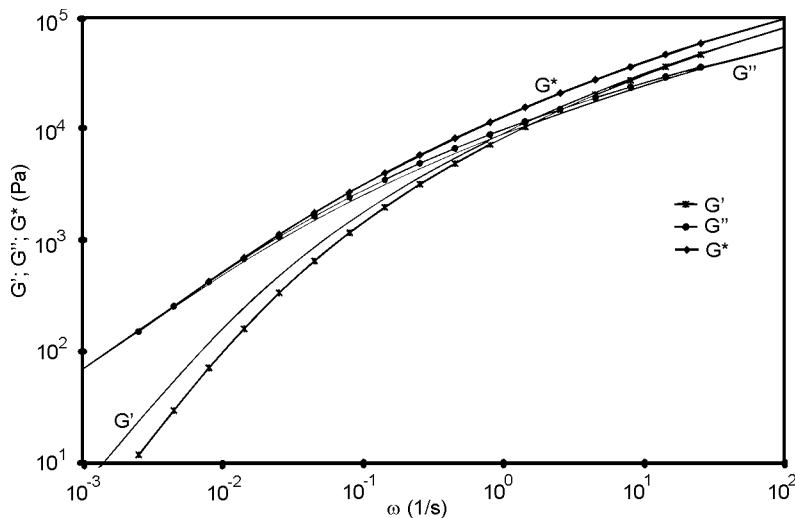


Figure 8. Measured data (shown by symbols) and modelled storage G' , loss G'' and complex G^* moduli for 1840H LDPE (a modern version of IUPAC A) at 200°C. Similar results were obtained at higher temperatures, but the discrepancy between G' and G'' increased at lower temperatures. There were no obvious difference between measured and modelled G^* and the complex viscosity.

The simulations revealed an odd phenomena: at temperatures from 190°C to 250°C the simulated data matched the measured data well, and crossing point was at 5/s for both procedures as shown in Fig. 8; whereas at lower temperatures down to 130°C the crossing points were not generated in the simulations since the modelled G' was much less than the measured G' . As discussed in our previous paper [8], software uses accurate values of the complex viscosity η^* and modulus G^* , for which there were no visible differences. That is why only complex data were used to detect the MWD. This might be due to the relaxation in some part of storage modulus G' being detected as loss modulus G'' . These error and discrepancies could be corrected by development new measurement methods.

3.3. Simulations for orientation level

Since the modelled and measured MWDs are related to molecular orientations at different deformations, we can use the principle reported by Borg *et al.* [9] to model orientation during flows and for final end products, where a high degree of orientation can cause warping and dimensional deviations over time. This would simultaneously provide accurate and complete pressure data, and an explanation for the entrance effects. Also, the filling phases of high-speed injection moulding could be simulated based on measured data, which is not possible by other ways using the original measured viscosity data for 1840H LDPE.

This information was used for capillary simulations using finite element modelling (FEM). Figure 9 shows the orientation in a 30L/D capillary tube, whose cross section was divided into five tubular layers of different diameters for FEM. FEM was performed using *cmv6* simulation software, which stores the shear history and orientation for all grid elements in old $\hat{P} \% = 100 \hat{P}(\dot{\gamma})$ values. Before performing the new data request, *cmv6* computes time step t , new pressure P , temperature T and imposed shear rate $\dot{\gamma}$ for all the finite elements. *DataPower* (a server-based program) supplies every element in *cmv6* (a client program) the new transient viscosity and $\hat{P} \%$ value to store in memory. Data transfers for the elements are performed via a small open-source DLL program communicating with the client and server as follows:

$$\text{Client: } (t, P, T, \dot{\gamma}, \hat{P} \%) \Rightarrow \text{Server: } (\hat{P} \%, \hat{\eta})$$

where Server computes the new effective orientation $\hat{P} \%$ and viscosity $\hat{\eta}$ for every element, and sends the new data to the *cmv6* program.

We found that a certain transition time is needed before the orientation reaches its new steady-state value at a higher shear rate in the capillary, and during relaxation in the polymer element after the capillary is withdrawn. The influence of pressure is not included so as to better illustrate the transient effects.

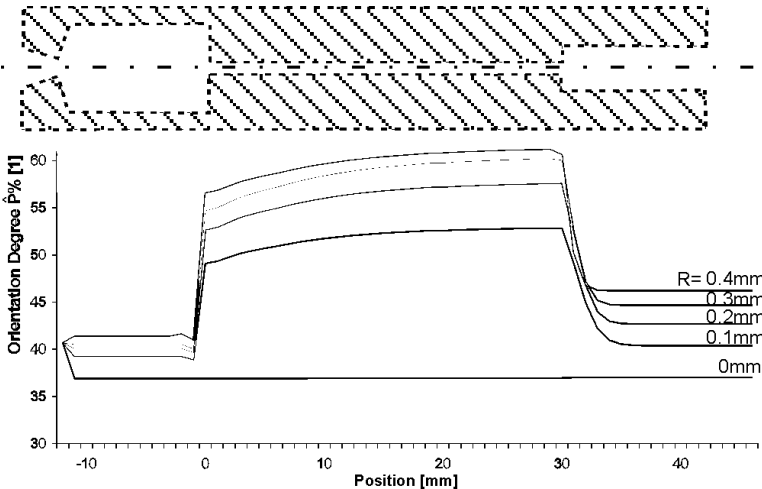


Figure 9. Orientation simulation for different layers in a 30L/D capillary tube at 150°C.

\hat{P} % values showing the degree of layer orientation as a function of radius and position in a capillary tube (illustrated at the top of the figure).

The orientation for a mobile-phone cover during the filling phase of injection moulding at one layer is shown in Fig. 10 in colour, where regions with higher \hat{P} % values are darker (where the orientation was also higher). The filling was complete in 0.3 s, and there was nonhomogeneous turbulence in the orientation at $t=0.1$ s during the filling phase (as shown in Fig. 10). It appeared that the melt flow was labile at high shear rates on the order of at least 10000/s. The orientation results were similar at different filling rates, but relaxation was evident close to the front surface. Further differences in the orientation level were evident in different layers, less in the top and bottom layers and more in the middle layers. The presence of a high residual orientation level in a completed cover can result in

warping, and such pieces cannot be used in the final phone assembly due to dimensional deviations.

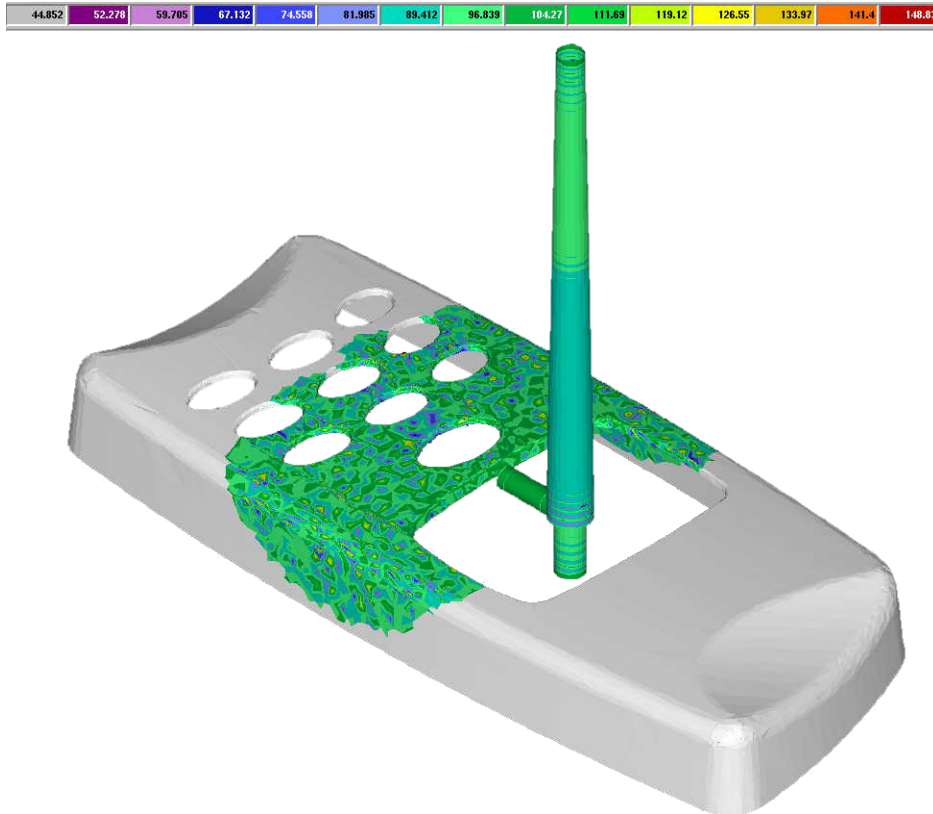


Figure 10. Orientation simulation layer at $t=0.1$ s during the filling of an injection mould for a mobile-phone cover. Different coloured regions and respective P -values/100 indicate orientation levels in the filled melt.

The combination of accurate complex viscosity measurements from an oscillating rheometer with capillary measurements can be used to generate complete analytical data. This offers more accurate simulations of pressure and the degree of orientation, which is related to the shrinkage and warpage of injection-moulded parts. Even though the results presented here fit well with practice, they are preliminary and hence further analyses are required.

4. Conclusions

We have modelled transient viscosity $\eta(t, \dot{\gamma})$ as a function of time starting from the MWD, and also described effective shear rate $\hat{\gamma}$ and respective effective viscosity $\hat{\eta}$ in the shear history of a polymer melt. These results were used to model start-up viscosity $\eta^+(t, \dot{\gamma})$ with an overshoot, according to measurements. The cessation after shear $\eta^-(t, \dot{\gamma})$ and realistic effective relaxation modulus depending on the shear history were modelled in a similar way. All of the results were consistent with measurements, and moreover our modelling technique can be applied of a very wide range of values that cannot be measured. One reason for the good results is the use of our new time-rate separability basis for functions instead of the normally used time-strain separability, which is violated in short-time responses.

The study has shown that shear viscosity is not only a viscometric function but also linearly viscoelastic. Similarly, the general Cox-Merz relations have been verified starting from the MWD and power-law formulas, and also the reasons for probable discrepancies have been presented. Factors of practical importance to viscosity measurements are demonstrated, such as why frequency-sweep measurements with an oscillation rheometer must be performed with upward-sweeping frequencies for well-relaxed samples in many cases, and why the measured storage G' and loss modulus G'' are not always reliable, whereas complex moduli G^* or viscosity η^* are.

The developed models can simulate not only the pressure losses in capillaries and when filling injection-moulding cavities, but also the molecular orientation and possible dimensional deviations of end products.

Acknowledgments

The orientation level was studied as part of EU research project VIM (Virtual Injection Molding). We thank Simcon Kunststofftechnische Software for providing the *cmv6* software and Mr Kimmo Ilen (Elastopoli) for converting the orientation chart for the mobile-phone cover. We also thank all partners of VIM.

References

- [1] D. W. Mead, R. G. Larson, M. Doi, A molecular theory for fast flows of entangled polymers, *J. Rheol.* 31 (1998) 7895-7914.
- [2] G. Marrucci, N. Grizzuti, Fast flows of concentrated polymers: Predications of the tube model of chain stretching, *Gazz. Chim. Ital.* 118 (1988) 179-185.
- [3] D. S. Pearson, A. D. Kiss, L. J. Fetters, M. Doi, Flow-induced birefringence of concentrated polyisoprene solutions, *J. Rheol.* 33 (1989) 517-535.
- [4] P. Rubio, M. H. Wagner, LDPE melt rheology and the pom-pom model, *J. Non-Newtonian Fluid Mech.* 92 (2000) 245–259.
- [5] G. Ianniruberto, G. Marrucci, A simple constitutive equation for entangled polymers with chain stretch, *J. Rheol.* 45 (2001) 1305-1318.
- [6] M. W. Collis, A. K. Lele, M. R. Mackley, R. S. Graham, D. J. Groves, A. E. Likhtman, T. M. Nicholson, O. G. Harlen, T. C. B. McLeish, L. R. Hutchings, Constriction flows of monodisperse linear entangled polymers: Multiscale modeling and flow visualization, *J. Rheol.* 49 (2) (2005) 501-522.

- [7] T. Borg, E. J. Pääkkönen, Linear viscoelastic models: Part I. Relaxation modulus and melt calibration, *J. Non-Newtonian Fluid Mech.* (2008), doi:10.1016/j.jnnfm.2008.07.011.
- [8] T. Borg, E. J. Pääkkönen, Linear viscoelastic models: Part II. Recovery of the molecular weight distribution using viscosity data, *J. Non-Newtonian Fluid Mech.* (2008), doi:10.1016/j.jnnfm.2008.07.010.
- [9] T. Borg, M. Keinonen, P. Poranen, E. J. Pääkkönen, in J. W. Lee and S. J. Lee (Eds.), Time dependency of viscosity in the flow simulations, *Proc. XIVth Int. Congr. on Rheology*, The Korean Society of Rheology, Seoul, Korea, 22-27 August 2004, CR24.
- [10] W. P. Cox, E. H. Merz, Correlation of Dynamic and Steady State Flow Viscosities, *J. Polym. Sci.* 28 (1958) 619-622.
- [11] J. M. Dealy, Official nomenclature for material functions describing the response of a viscoelastic fluid to various shearing and extensional deformations, *J. Rheol.* 39 (1995) 253-265.
- [12] Y. Kwon, K. S. Cho, Time-strain nonseparability in viscoelastic constitutive equations, *J. Rheol.* 45 (2001) 1441-1452.
- [13] J. Meissner, Basic parameters, melt rheology, processing and end-use properties of three similar low-density polyethylene samples, *Pure and Appl. Chem.* 42 (1975) 551-662.
- [14] J. Meissner, Modifications of the Weissenberg Rheogoniometer for measurement of transient rheological properties of molten polyethylene under shear. Comparison with tensile data, *J. Appl. Polymer Sci.* 16 (1972) 2877-2899.
- [15] H. M. Laun, Pressure dependent viscosity and dissipative heating in capillary rheometer of polymers melts, *Rheol. Acta* 42 (2003) 295-308.

[16] C.M. Roland, C. G. Robertson, Recovery of shear-modified polybutadiene solutions, Rubber Chem Tech. 79 (2006) 267-280.